Combustion and Flame 159 (2012) 1417–1425

Contents lists available at SciVerse ScienceDirect

Combustion and Flame

journal homepage: www.elsevier.com/locate/combustflame

Laminar flame speeds of cyclohexane and mono-alkylated cyclohexanes at elevated pressures

Fujia Wu, Andrew P. Kelley, Chung K. Law *

Department of Mechanical and Aerospace Engineering, Princeton University, Princeton, NJ 08544, USA

ARTICLE INFO

Article history:
Received 26 October 2011
Received in revised form 19 November 2011
Accepted 20 November 2011
Available online 10 December 2011

Keywords:
Laminar flame speeds
Elevated pressures
Cyclo-alkanes
Naphthenes
Mono-alkylated cyclohexanes
Fuel surrogates

ABSTRACT

The propagation speeds of expanding spherical flames of cyclohexane, methylcyclohexane and ethylcyclohexane in mixtures of oxygen/inert were measured in a heated, dual-chamber vessel, with the corresponding laminar flame speeds extracted from them through nonlinear extrapolation. Measurements were conducted at atmospheric and elevated pressures up to 20 atm. Computational simulations were conducted using the JetSurF 2.0 mechanism, yielding satisfactory agreement with the present measurements at all pressures, with a slight over-prediction at 1 atm. Measurements reveal the following trend for the flame speeds: cyclohexane > *n*-hexane > methylcyclohexane ≈ ethylcyclohexane at all pressures, with the maximum difference being approximately 5% at 1 atm and 13% at 10 atm. Examination of the computed flame structure shows that owing to its symmetric ring structure, decomposition of cyclohexane produces more chain-branching 1,3-butadiene and less chain-terminating propene. On the contrary, a more balanced distribution of intermediates is present in the flames of methylcyclohexane and ethylcyclohexane due to substitution of the alkyl group for H.

1. Introduction

Cyclo-alkanes are components of commercial fuels such as jet fuel which typically has around 20% of cyclo-alkanes by volume [1]. Some alternative fuels, particularly those derived from coal [2], are almost entirely composed of cyclo-alkanes. However, the combustion characteristics and oxidation kinetics of cyclo-alkanes have not been studied as extensively as *n*-alkanes.

There have been relatively few measurements of the laminar flame speeds for cyclo-alkanes. Most data were obtained at atmospheric or slightly elevated pressures. Specifically, Davis and Law [3] measured the laminar flame speeds for cyclohexane and cyclopentane at atmospheric pressure and unburned gas temperature of 298 K; Farrell et al. [4] measured those of cyclohexane, cyclopentane, and methylcyclopentane at 3 atm and 450 K; Dubois et al. [5] measured those of *n*-propylcyclohexane at 403 K and atmospheric pressure; and Ji et al. [6] measured those of cyclohexane, methyl-, ethyl-, *n*-propyl- and *n*-butyl-cyclohexanes at 353 K and atmospheric pressure.

Cyclohexane and its mono-alkylated derivatives have been selected as representative cyclo-alkane components of surrogate jet fuels [2], gasoline [7] and diesel [8]. Several kinetic models have been proposed, such as the semi-detailed models for cyclohexane and methylcyclohexane by Ranzi and co-workers [9–11], the kerosene model by Dagaut and co-workers [12] which includes the kinetics of cyclo-alkanes, and Westbrook and co-workers' models for cyclohexane and methylcyclohexane [13,14]. Recently, a detailed high-temperature model, JetSurF 2.0 [15], has been developed which includes the kinetics of cyclohexane and mono-alkylated cyclohexanes. The performance of JetSurF 2.0 in predicting the laminar flame speeds of cyclohexane and mono-alkylated cyclohexanes has been well validated at atmospheric pressure in [6]; however, its performance at elevated pressures has not been evaluated.

The fundamental understanding on the decomposition and further oxidation of cyclo-alkanes is also of interest. Studies of the laminar flame speeds of C_5–C_8 alkanes [3,16,17] showed that they are almost identical. The reason for this fuel similarity has been attributed [17] to the fact that *n*-alkanes all crack into similar small fragments (C_0–C_4) in flames due to their similar straight-chain molecular structure. However, this fuel similarity does not seem to exist for cyclo-alkanes from the measurements of Ji et al. [6], in which the following trend was found for the flame speeds: cyclohexane > *n*-hexane > mono-alkylated cyclohexanes. Using numerical simulation, Ji et al. [6] attributed the difference between *n*-hexane and cyclohexane to thermal effects, *i.e.*, the small difference in the adiabatic flame temperatures, and the difference between cyclohexane and its mono-alkylated derivatives to chemical kinetic effects caused by the change in the distribution of smaller molecules formed when the original fuel molecules decompose. In particular, mono-alkylated cyclohexane was found to form more propene while

* Corresponding author.
E-mail address: cklaw@princeton.edu (C.K. Law).

0010-2180/$ - see front matter © 2011 The Combustion Institute. Published by Elsevier Inc. All rights reserved.
doi:10.1016/j.combustflame.2011.11.012

cyclohexane more 1,3-butadiene. The former would lead to chain terminating reactions while 1,3-butadiene would lead to chain branching, resulting in a lower flame speed for the mono-alkylated cyclohexanes as opposed to cyclohexane.

The present study aims to provide archival laminar flame speed data for cyclohexane, methylcyclohexane and ethylcyclohexane at pressures from 1 atm to 20 atm at the initial temperature of 353 K. These measurements will allow us to investigate the pressure effect on the flame propagation of cyclohexane and its mono-alkylated derivatives; for instance whether the effect of alkyl group substitution on the laminar flame speed still holds at elevated pressures. Furthermore, substantial data at various conditions also allow for further understanding of the thermal decomposition and oxidation of cyclo-alkanes.

2. Experimental specifications

2.1. Experimental setup

Laminar flame speeds were determined using expanding spherical flames. Since detailed descriptions and dimensions of the experimental apparatus, procedure and data analysis were reported in two previous publications [17,18], only a brief description of the experimental apparatus and procedure is provided here.

The apparatus consists of a cylindrical chamber radially situated within another cylindrical chamber of substantially larger volume. The wall of the inner chamber is fitted with a series of holes that can be mechanically opened and closed to allow the union and separation of the gases in the inner and outer chambers. The outer chamber is covered with silicon electrical heaters, hence enabling it to act as an oven to uniformly heat the inner chamber to a given temperature, which is 353 K and is the initial gas temperature for all of the present data.

The experimental procedure involves first filling the inner chamber with fuel vapor produced by heating a liquid fuel reservoir maintained at 353 K, followed by a certified mixture of oxidizer and inert gas which is also preheated to at least 353 K. The desired equivalence ratio in the inner chamber is obtained by monitoring the partial pressures of the gases in the inner chamber. The outer chamber is filled with a mixture of inert gases to match the pressure and density of the gas in the inner chamber.

After filling the inner and outer chambers, the inner chamber gases are thoroughly mixed using a series of fans and pumps to ensure homogeneity. The gas is then allowed to settle briefly before it is spark ignited. Concurrent to this instant, the holes between the inner and outer chambers are opened, resulting in an expanding spherical flame that propagates throughout the inner chamber in essentially an isobaric environment before it is quenched upon contacting the inert gases of the outer chamber. The flame surface is visualized using a pin-hole Schlieren system coupled to a high-speed camera running typically at 10,000 frames per second.

As a secondary check of the gas composition in the inner chamber, samples of the gas in the tubing connected to the inner chamber are analyzed using a gas chromatograph with a flame ionization detector. All gas samples were verified to have less than a 2% random error in the equivalence ratio, as is expected based on the gas filling procedure.

2.2. Data analysis

Tracking the flamefront yields the history of the radius of the spherical flame as a function of time, $r_f(t)$. For extrapolation of the laminar flame speed from $r_f(t)$, the relation recently derived by Kelley et al. [19] is employed,

$$S_b^0 t + C = r_f + 2L_b \ln r_f - \frac{4L_b^2}{r_f} - \frac{8L_b^3}{3r_f^2} \tag{1}$$

where S_b^0 is the adiabatic, unstretched gas speed of the burned mixture relative to the flame, r_f the flame radius, L_b the Markstein length, t the time and C a constant accounting for the initial conditions. With S_b^0 the laminar flame speed, S_u^0, can then be calculated from the continuity relation,

$$\rho_u^0 S_u^0 = \rho_b^0 S_b^0 \tag{2}$$

where ρ_u^0 and ρ_b^0 are respectively the densities of the unburned and burned mixtures. It is noted that Eq. (1) contains up to the third-order accuracy in terms of the inverse flame radius. Other extrapolation relations, such as the linear model [20], nonlinear model with quasi-steady approximation [21] and the Markstein's empirical equation [22] only contain up to first or second order accuracy. While the flame speeds extrapolated from the linear model [20] are generally higher than that from the quasi-steady nonlinear model [21], for both $Le > 1$ and $Le < 1$ cases, using Eq. (1) leads to results between the two, and is much closer to those of the latter [21]. For typical hydrocarbon fuels, using Eq. (1) and the quasi-steady nonlinear relation [21] leads to a maximum difference of only approximately 1 cm/s, with the difference increasing as the equivalence ratio deviates from the value corresponding to zero Markstein number.

We further note that for flame speed measurements using expanding spherical flames, the data selected for extrapolation need to be in a certain radius range in that the small and large radius data are respectively contaminated by the influences of ignition and the chamber confinement, as discussed in details in [23–26]. For our experimental setup and the choice of fuels studied, a conservative assessment of this range is between radii of 1.0 and 1.8 cm. The actual selected data for extrapolation at each data point was within this range, assisted by assessment of the trajectories of dr_f/dt versus stretch rate, $(2/r_f)dr_f/dt$. Based on repeated measurements and the sensitivity of slight variation of the data selection, all reported laminar flame speeds in this paper have an uncertainty of approximate ±2 cm/s.

2.3. Numerical approach

For quantitative comparison and mechanism studies, numerical computation was performed using the Chemkin Premix code [27] to determine the computed laminar flame speeds as well as detailed flame structure. All calculations used multi-component formulation for transport properties including Soret diffusion. The calculation used finite difference method with adaptive gridding, which was refined until a grid-independent solution was found.

The present study uses the JetSurF 2.0 mechanism developed by Wang et al. [15], which includes 348 species and 2163 reactions. There are also other existing mechanisms [9–14]; however, since the focus of the paper is on providing experimental data, JetSurF 2.0 was selected as an example for comparison. Indeed, it is also the only mechanism that can simulate the combustion of ethylcyclohexane so far.

3. Results

3.1. Validation of present approach

In order to assess the validity of the present approach, we shall first compare the laminar flame speeds with those in the literature. For n-heptane at atmospheric pressure, which has been extensively studied in the literature, four independent measurements can be used for comparison: the data of Kelley et al. [17] obtained using

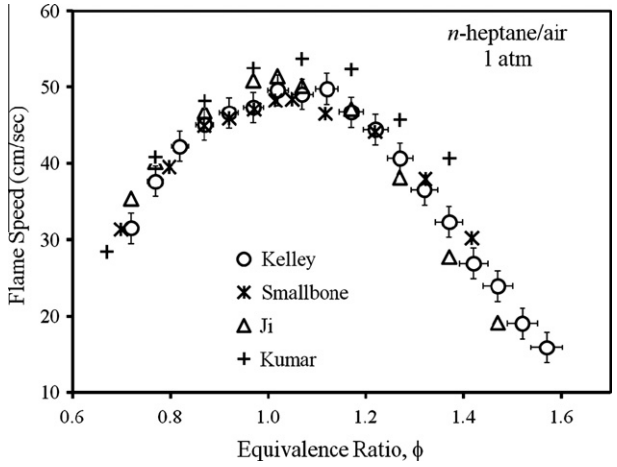

Fig. 1. Comparison of laminar flame speeds of *n*-heptane/air at atmospheric pressure. Data include: Kelly et al. [17] (T_u = 353 K), Smallbone et al. [28] (T_u = 350 K), Ji et al. [16] (T_u = 353 K) and Kumar et al. [29] (T_u = 360 K). A correction of $S_u^0 \sim T_u^{1.8}$, as suggested by numerical predictions with the JetSurf 2.0 mechanism, was employed on the data of Smallbone et al. [28] and Kumar et al. [29] to account for the small difference in the initial temperatures from 353 K.

the present experimental set-up, and the counterflow data of Ji et al. [16], Smallbone et al. [28] and Kumar et al. [29]. The data of Kelley et al. [17] has been re-analyzed using Eq. (1) for extrapolation. The resulting comparison is plotted in Fig. 1. It is seen that except for the data of Kumar et al. [29] which show consistently higher values, the other three measurements are in relatively close agreement. The difference between the measurements of Kelley et al. [17] and Smallbone et al. [28] is the smallest in spite of the difference in the experimental approaches. There is a slightly "lean-shift" between measurements of Ji et al. [16] and Kelley et al. [17]: the former peaks at $\phi \approx 1.05$ while the latter peaks at $\phi \approx 1.1$. This discrepancy, although small, is out of the range of the experimental error and has consistently appeared in the data for other normal alkanes reported by the two groups [16,17]. The source of this disagreement is yet to be determined. Furthermore, based on the present comparison as well as those in the literature, the data of Kumar et al. [29] appear to carry substantial though unquantified error, and as such may need to be excluded in future comparisons.

3.2. Results with air as oxidizer

Using air from a certified cylinder of 21 mol% O_2/79 mol% N_2 as the oxidizer, laminar flame speeds were determined up to 10 atm in pressure. The complete sets of data on the laminar flame speeds of cyclohexane, methylcyclohexane and ethylcyclohexane are shown in Fig. 2, for pressures of 1, 2, 5, and 10 atm, except for ethylcyclohexane for which saturation starts at 10 atm. For each pressure, the lean limit was such that the ignition energy available was not able to drive the flame beyond the critical radius required for successful flame initiation [23]. The rich limit for atmospheric pressure experiments was due to the onset of buoyancy effects when the flame speed is substantially reduced, while those at higher pressures were due to the onset of flamefront cellular instability.

Experimental data of Ji et al. [6] as well as the corresponding predictions of the JetSurF 2.0 mechanism are also plotted in Fig. 2 for comparison. Comparing the present measurements to those of Ji et al. [6], we see generally close agreement. However, their data tend to be slightly higher on the lean side and slightly lower on the rich side, a similar trend found in the comparison between data from the two groups for C_5–C_8 *n*-alkanes [16,17].

In comparison with the chemical kinetic predictions of JetSurF 2.0, it is seen that for all pressures the largest disagreement turns

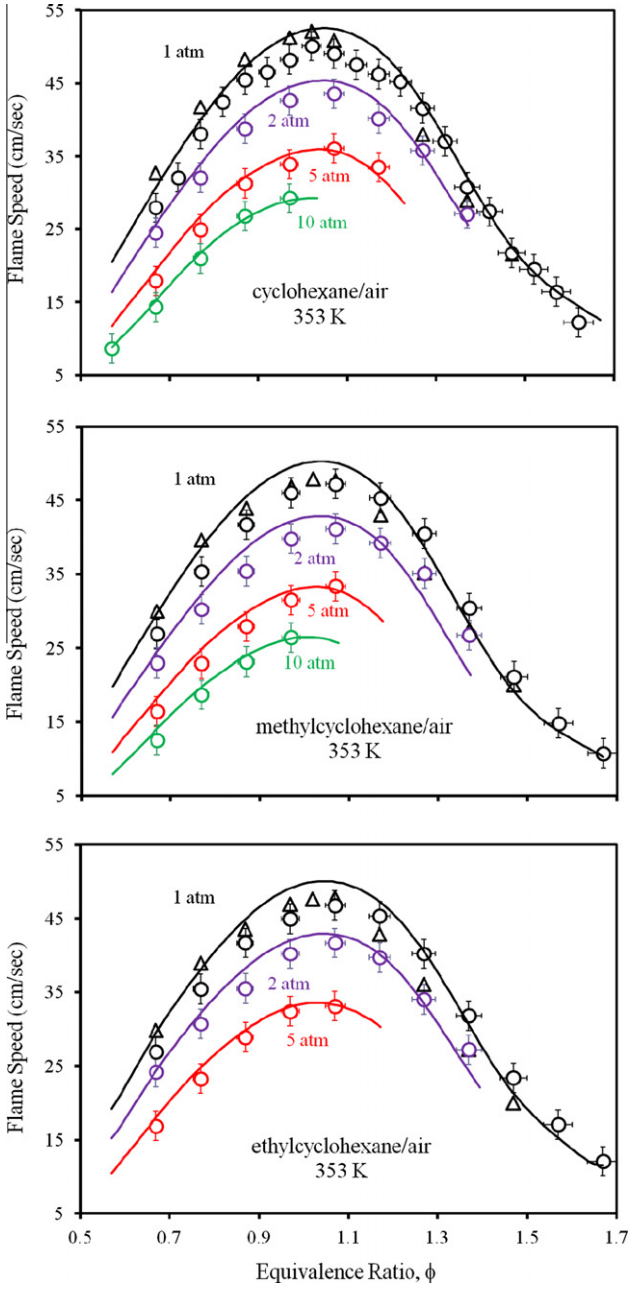

Fig. 2. Laminar flame speeds of cyclohexane, methylcyclohexane and ethylcyclohexane at various pressures with air as the oxidizer, unburned gas temperature of 353 K. Circles: present measurements; Triangles: measurements of Ji et al. [6]; Solid lines: computed values using JetSurF 2.0 mechanism [15].

out to be at atmospheric pressure. The mechanism generally agrees quite well at elevated pressures with differences less than 3%. However, at atmospheric pressure there is a maximum difference of 6%, 8% and 7% for cyclohexane, methylcyclohexane and ethylcyclohexane, respectively. The peak values in the flame speeds are over-predicted for all three fuels, and there is also a slight shift in the peak locations to the lean side. Nevertheless, the overall agreement between measurements and model predictions at all pressures indicates adequate performance of the mechanism in predicting the laminar flame speeds.

3.3. Results with oxygen/helium as oxidizer

In order to measure the flame speeds at pressures higher than 10 atm, a mixture of 15 mol% O_2 with 85 mol% He was used in

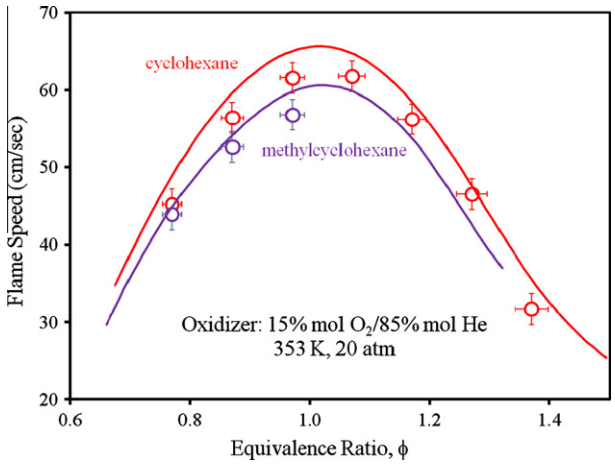

Fig. 3. Laminar flame speeds of cyclohexane, methylcyclohexane with O_2/He mixture (15:85) as the oxidizer, at 20 atm unburned gas temperature of 353 K. Solid lines: computed values using JetSurF 2.0 mechanism [15].

place of air. The use of helium in place of nitrogen results in a larger Lewis number for the mixture such that diffusional-thermal instabilities are more readily suppressed [26]. Additionally, decreasing the oxygen concentration results in an increase in the flame thickness. This tends to suppress the hydrodynamic instability which becomes progressively more prominent with increasing pressure.

The laminar flame speeds of cyclohexane and methylcyclohexane at 20 atm are plotted in Fig. 3, along with the corresponding predictions by JetSurF 2.0. The absence of data for methylcyclohexane on the rich side and for ethylcyclohexane was due to fuel vapor saturation at those conditions. Although with reduced oxygen concentration, the laminar flame speeds at 20 atm are much higher than those with air as the oxidizer at 10 atm due to the low specific heat and high conductivity of helium.

Comparing the present measurements to the predictions of JetSurF 2.0, it is seen that the mechanism generally agrees quite well for methylcyclohexane, with maximum difference being less than 3%. However, there is a uniform slight over-prediction for cyclohexane, with a maximum difference of 6%, which is higher than the difference between measurements and predictions at 10 atm with air as the oxidizer.

4. Comparison and discussion

4.1. Comparison of flame speeds

The laminar flame speeds of cyclohexane, methylcyclohexane and ethylcyclohexane determined at all conditions in the present study are compared with those of *n*-hexane in Fig. 4. The data of *n*-hexane are taken from [17] and have been re-analyzed using Eq. (1) for extrapolation.

While almost identical flame speeds have been found for C_5–C_8 alkanes [17], this is not the case for cyclo-alkanes as seen in Fig. 4. Compared to *n*-hexane, flame speeds of cyclohexane are uniformly higher except for the very rich conditions at 1 atm. The laminar flame speeds of methylcyclohexane and ethylcyclohexane are almost identical but uniformly lower than those of *n*-hexane. This result agrees with the trends found in Ji et al. [6] at atmospheric pressure. Furthermore, the present measurements show that the same trend can be extended to elevated pressures.

To identify the pressure effects more clearly, we plot the percentage difference in the maximum flame speed between different fuels in Fig. 5. It is seen that the difference in flame speeds between

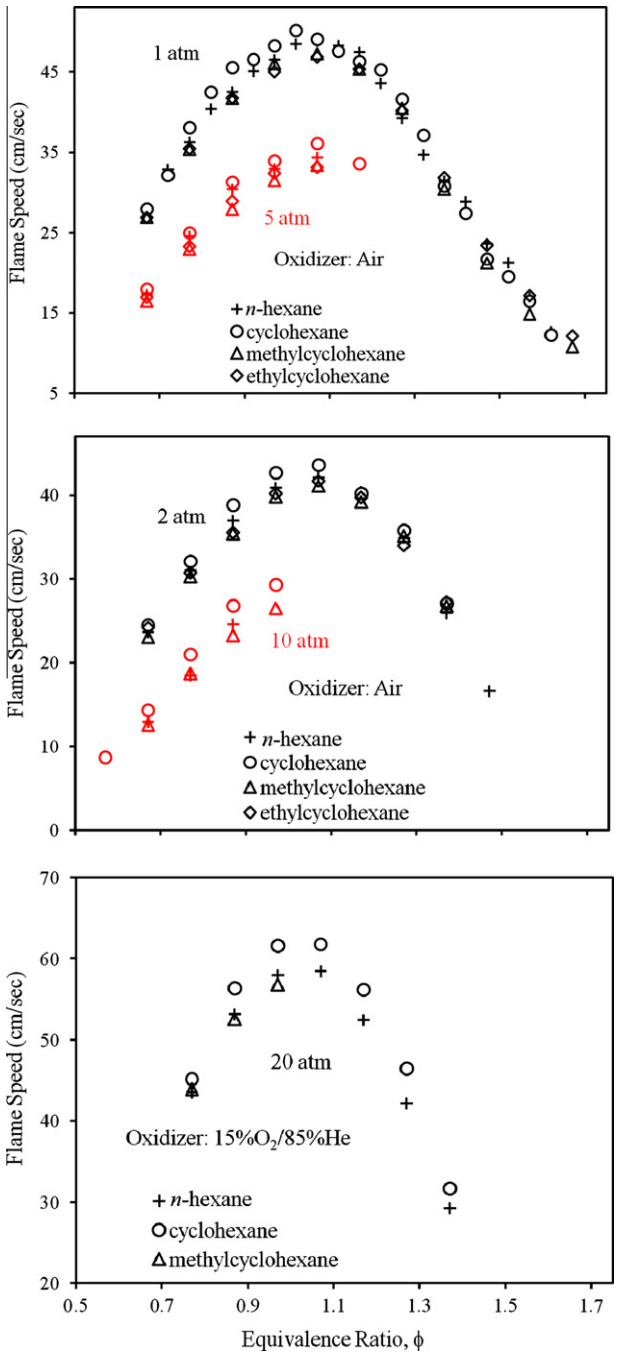

Fig. 4. Comparison of measured laminar flame speeds of *n*-hexane, cyclohexane, methylcyclohexane and ethylcyclohexane at various pressures with initial temperature of 353 K.

cyclohexane and *n*-hexane becomes larger as pressure increases. The percentage difference increases from approximately 2% to 10% as the pressure increase from 1 to 10 atm. The difference in flame speeds between *n*-hexane, methylcyclohexane and ethylcyclohexane, however, is insensitive to pressure, remaining at approximately 3% from 1 atm to 10 atm. Consequently, the difference in flame speeds between cyclohexane and its mono-alkylated counterparts increases from approximately 5% at 1 atm to 13% at 10 atm.

The trend in flame speeds between different fuels observed experimentally is well captured by simulations with JetSurF 2.0, as shown in Fig. 6. This means that the underlying mechanism

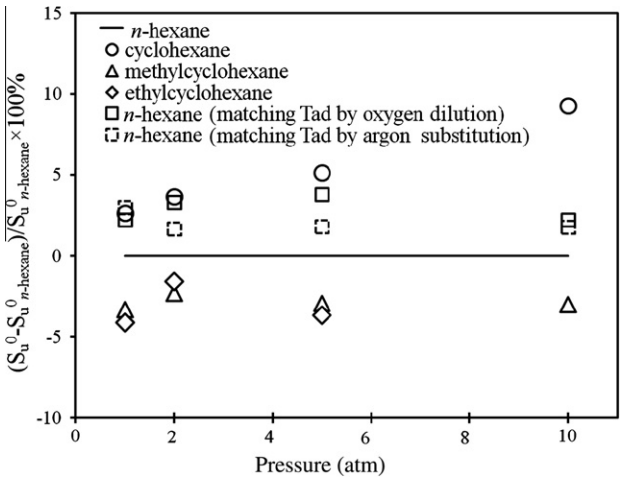

Fig. 5. Percentage difference in the maximum flame speed between *n*-hexane/air, cyclohexane/air, methylcyclohexane/air and ethylcyclohexane/air mixtures versus pressures with unburned gas temperature of 353 K.

responsible for the difference in the flame speeds between different fuels is possibly contained in the mechanism.

4.2. Thermal effects

The present measurements, those of Ji et al. [6], and the predictions by JetSurF 2.0 mechanism all consistently show the following trend for the laminar flame speeds: cyclohexane > *n*-hexane > methylcyclohexane ≈ ethylcyclohexane, which behooves us to seek the fundamental reasons governing this ordering.

We shall first investigate the thermal properties of the fuels. Figure 7 plots the adiabatic flame temperature of the fuel/air mixtures at atmospheric pressure; the adiabatic flame temperatures at elevated pressures show the similar trend. From Fig. 7, it is seen that cyclohexane, methylcyclohexane and ethylcyclohexane have almost the same adiabatic flame temperature. However, the adiabatic flame temperature of *n*-hexane is lower than the other three fuels by approximately 10 K. This result is reasonable because while cyclohexane, methylcyclohexane and ethylcyclohexane have C/H ratio of 0.5, *n*-hexane has the value of 0.43. Since all fuels in the present study have no double, C=C bond, the dominant parameter is then the C/H ratio, with flame temperature increasing with the C/H ratio.

By numerically making the flame temperature of *n*-hexane equal to that of cyclohexane, achieved by substituting part of the inert, nitrogen, by argon, Ji et al. [6] found that the resulting flame speed of *n*-hexane becomes basically the same as that of cyclohexane, hence implying that the cause of the difference in the flame speeds is thermal in nature. In view of this important insight, we have extended the investigation of Ji et al. [6] along two directions. First, we have repeated the calculation using the same inert substitution method, in which about 2.8 mol% of N_2 is substitute by Ar, and alternatively we have also replaced part of N_2 by O_2, such that the O_2 concentration is increased from 21.0 to 21.2 mol%. Second, we have performed the investigation to pressures higher than 1 atm, which is the pressure studied in Ji et al. [6].

Figure 5 shows that the increases in the flame speed using both methods of flame temperature matching are basically the same, hence provides mutual support to the validity of the two methods of flame-temperature matching. Furthermore, while our result substantiates that of Ji et al. [6] at 1 atm, increasingly larger differences in the flame speeds of *n*-hexane and cyclohexane are observed as the pressure increases. For example, matching the flame temperatures at 10 atm increases the flame speed of *n*-hexane by only about 2%, such that the flame speed of cyclohexane is still 8% higher than that of *n*-hexane at this pressure. This result therefore suggests that thermal effect cannot completely explain the difference in the flame speeds between *n*-hexane and cyclohexane.

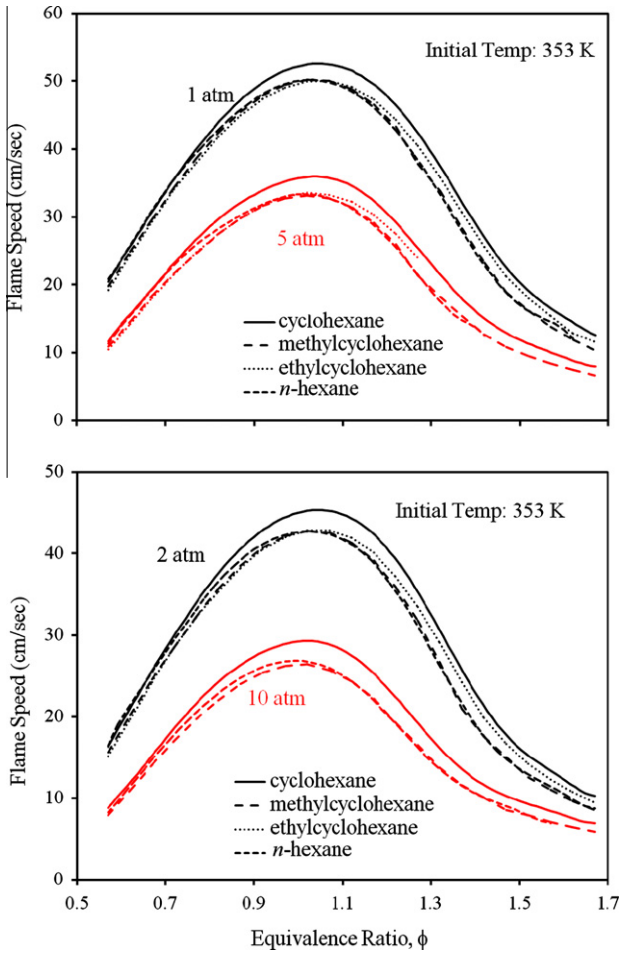

Fig. 6. Comparison of predicted laminar flame speeds of *n*-hexane, cyclohexane, methylcyclohexane and ethylcyclohexane by JetSurF 2.0 mechanism [15] at 1, 2, 5 and 10 atm with air as oxidizer at unburned gas temperature of 353 K.

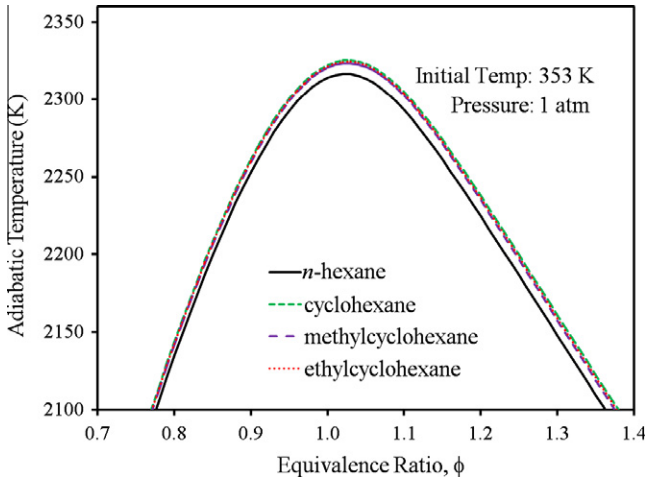

Fig. 7. Comparison of adiabatic flame temperatures of *n*-hexane, cyclohexane, methylcyclohexane and ethylcyclohexane at atmospheric pressure. Thermodynamic data in JetSurF 2.0 mechanism [15] was used in the calculation.

It is also seen from Figs. 6 and 7 that the difference in flame speeds between cyclohexane, methylcyclohexane and ethylcyclohexane is not caused by the thermal effect as these three fuels have almost identical adiabatic flame temperatures. All these results then lead us to investigate possible effects due to intrinsic chemical kinetics, discussed next.

4.3. Kinetic effects

The transport properties of the above fuels are similar to those of C_6–C_8 *n*-alkanes, for which similar flame speeds have been found [17]. Therefore we shall next examine the disparities in flame structures and kinetic behaviors between the different fuels. Since JetSurf 2.0 yields fairly close agreement for different fuels in both the values and trends of the laminar flame speeds, it is therefore justified to use the mechanism to examine the flame structure numerically.

Figure 8 plots the temperature and heat release profiles for *n*-hexane, cyclohexane, methylcyclohexane and ethylcyclohexane for the 1-D premixed flames obtained from JetSurF 2.0 at 1 and 10 atm, and $\phi = 1.0$. It is seen that both the temperature and heat release profiles of *n*-hexane, methylcyclohexane and ethylcyclohexane are quite close, even though there is a slight difference in the flame temperatures at the equilibrium state. The temperature and heat release profiles of cyclohexane, however, deviate from those of the other three fuels. In particular, the temperature profile of cyclohexane is steeper than those of the other three fuels, corresponding to stronger heat release. In addition, the difference is intensified at 10 atm when compared to the case at 1 atm. As seen in Fig. 8, the heat release rate at 10 atm of cyclohexane is further increased. The maximum difference between the heat release rate of cyclohexane and the other fuels increases from 3% at 1 atm to 8% at 10 atm. With the adiabatic flame temperature being close, this difference in heat release clearly indicates a unique kinetic behavior of cyclohexane, compared to the other fuels.

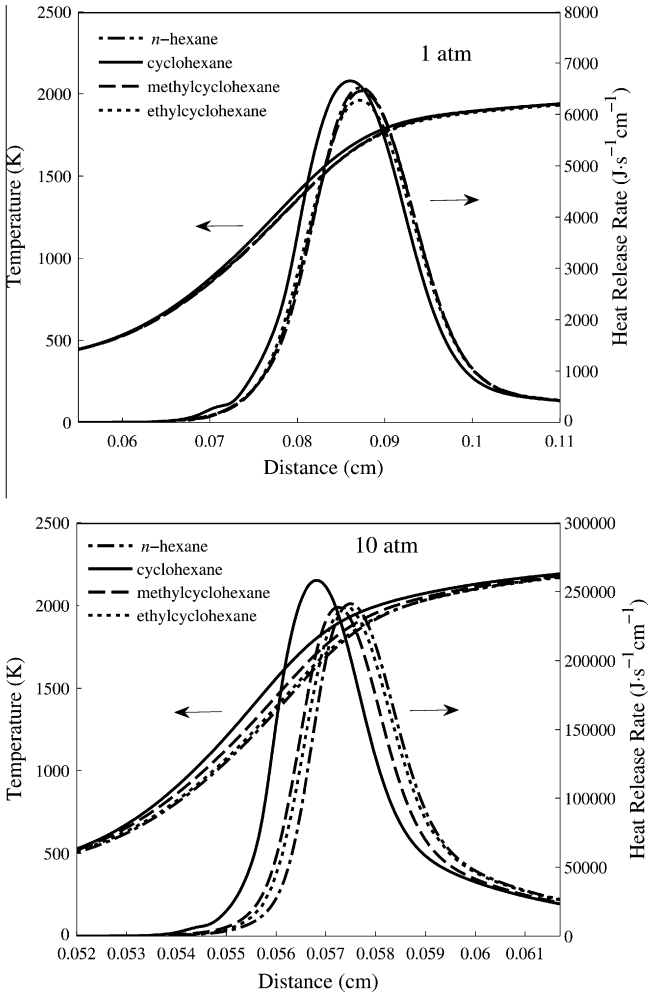

Fig. 8. Temperature and heat release profiles for the 1-D flames of *n*-hexane/air, cyclohexane/air, methylcyclohexane/air and ethylcyclohexane/air at $\phi = 1.0$, unburned gas temperature of 353 K, calculated with JetSurF 2.0 mechanism [15].

In several previous studies on the premixed flame structure of large-molecule fuels [6,16,17,30], it was suggested that the initial fuel cracking process to form small fuel fragment such as (CH_4, C_2H_4, *etc.*) and the oxidation of these fuel fragments can be decoupled. Furthermore, since the initial fuel cracking occurs relatively fast at temperatures above 1100 K, the oxidation of the fuel fragments mainly controls the heat release and eventually flame propagation. This is indeed true as seen from the sensitivity analysis of the rate constants in Figs. 9a–c for *n*-hexane/air, cyclohexane/air and methylcyclohexane/air mixtures at 1 and 10 atm, in which all the important reactions are those involving the oxidation of C_0–C_4 fuel fragments. Following this concept, we shall examine the major fuel fragments in flame structure and their importance in controlling the overall burning rate.

Figure 10 plots the profiles of the major C_0–C_4 fuel fragments in the flames of stoichiometric *n*-hexane/air, cyclohexane/air and methylcyclohexane/air mixtures at 10 atm. It is noted that the fragments shown in Fig. 10 not only have dominant concentrations but also participate in the important reactions identified through the sensitivity analysis. First, from Fig. 10 it is seen that the dissimilarity between different fuels increase as the carbon number of intermediates increases from 0 to 4. In particular, the profiles of H, OH, O and CO of different fuels are very similar, while the profiles of CH_3, CH_4, C_2H_2 and C_2H_4 show some extent of disparity but are still of the same order of magnitude. However, profiles of the major C_3 and C_4 intermediates, propene and 1,3-butadiene, show significant disparity between *n*-hexane, cyclohexane and methylcyclohexane. Similar to what Ji et al. [6] have found at atmospheric pressure, decomposition of cyclohexane forms considerably more 1,3-butadiene and less propene, compared to *n*-

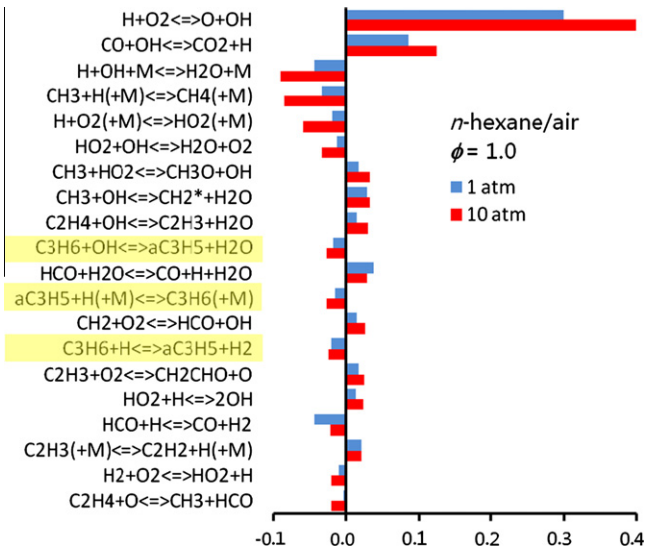

Fig. 9a. Normalized rate constant sensitivity coefficients on burning rate of *n*-hexane/air mixture, at $P = 1$, 10 atm, $\phi = 1.0$, unburned gas temperature of 353 K, calculated with JetSurF 2.0 mechanism [15]. The major different reactions from other fuels are highlighted in yellow. (For interpretation of the references to color in this figure legend, the reader is referred to the web version of this article.)

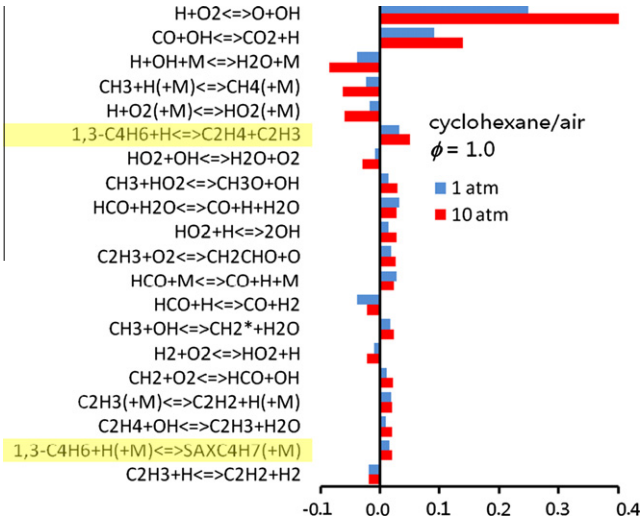

Fig. 9b. Normalized rate constant sensitivity coefficients on burning rate of cyclohexane/air mixture, at $P = 1$, 10 atm, $\phi = 1.0$, unburned gas temperature of 353 K, calculated with JetSurF 2.0 mechanism [15]. The major different reactions from other fuels are highlighted in yellow. (For interpretation of the references to color in this figure legend, the reader is referred to the web version of this article.)

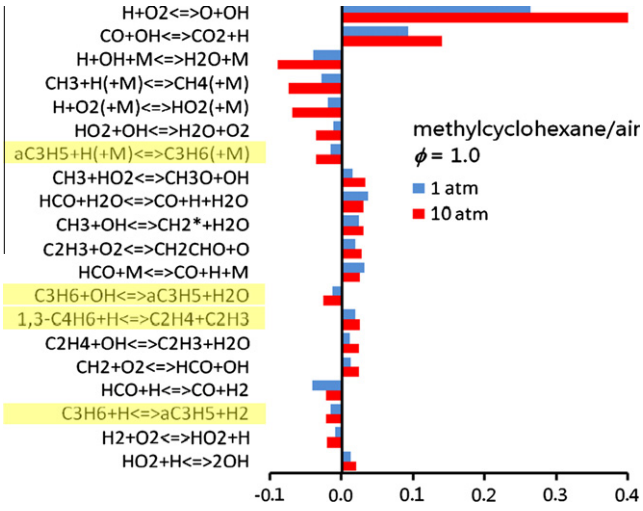

Fig. 9c. Normalized rate constant sensitivity coefficients on burning rate of methylcyclohexane/air mixture, at $P = 1$, 10 atm, $\phi = 1.0$, unburned gas temperature of 353 K, calculated with JetSurF 2.0 mechanism [15]. The major different reactions from other fuels are highlighted in yellow. (For interpretation of the references to color in this figure legend, the reader is referred to the web version of this article.)

hexane and methylcyclohexane: the peak concentration of propene for cyclohexane is 30% and 40% of those for *n*-hexane and methylcyclohexane, while the peak concentration of 1,3-butadiene for cyclohexane is 19 and 2 times those for *n*-hexane and methylcyclohexane. This dominant difference between the fractions of 1,3-butadiene and propene is shown in the following discussion to be mostly responsible for the difference in the global burning rates observed both experimentally and numerically.

The relatively low reactivity of propene and high reactivity of 1,3-butadiene were noted in [6]: the abstraction of H from propene through the reaction $C_3H_6 + H \rightarrow aC_3H_5 + H_2$ leads to aC_3H_5, which tends to react through $aC_3H_5 + H + M \rightarrow C_3H_6 + M$ to regenerate propene, leading to chain termination by forming a net sink for H. On the contrary, typical subsequent reactions of 1,3-butadiene break the single C—C bond, for example, $1,3\text{-}C_4H_6 + H \rightarrow C_2H_4 + C_2H_3$, the products of which also have high reactivity.

The difference in the kinetic behavior between 1,3-butadiene and propene can also be seen from results of the sensitivity analysis in Figs. 9a–c. Among the sensitivity coefficients for various reactions, it is seen that while the reactions involving H, CO and C_1–C_2 intermediates show similar importance for the three fuels, the major difference lies in the reactions involving 1,3-butadiene and propene. For *n*-hexane, the chain termination reactions involving propene and aC_3H_5 exhibit a notable influence, and as expected the influence is negative. For cyclohexane, however, none of the important reactions involve propene and aC_3H_5. This is because, in the flames of cyclohexane, there are not as many C_3 intermediates as in the flames of *n*-hexane; therefore the corresponding propene and aC_3H_5 reactions are not the rate-limiting steps anymore. Instead, the chain branching reactions involving 1,3-butadiene exhibit a notable positive influence, which is due to the high concentration of 1,3-butadiene in the flames of cyclohexane. Finally, for methylcyclohexane the sensitivity coefficients appear different from that for cyclohexane: the reactions involving propene and aC_3H_5 become important again, corresponding to a relatively higher concentration of propene in the flames of methylcyclohexane. From the above results, we therefore conclude that the higher flame speeds of cyclohexane as compared to those of the other fuels is due to its respectively higher and lower fraction of C_3 and C_4 species among all intermediates.

From Figs. 9 and 10, it is also seen that the different distribution of C_3–C_4 intermediates can explain the pressure effect seen in the heat release profiles and the laminar flame speeds. From the sensitivity analysis results, it is seen that the reactions involving C_3 and C_4 intermediates all have higher sensitivity coefficients at 10 atm compared to their values at 1 atm. This is because as pressure increases, there are more chain terminating third-body reactions, such as $aC_3H_5 + H + M \rightarrow C_3H_6 + M$. This fact aggravates the sensitivity of the dependence of the overall burning rate on the fuel fragment distribution. For example, considering the reactions $aC_3H_5 + H + M \rightarrow C_3H_6 + M$ and $aC_3H_5 + H \rightarrow aC_3H_4 + H_2$, calculation with JetSurF 2.0 shows that the ratio of the maximum reaction rates of the two reactions respectively increase from 7.2 at 1 atm, to 8.1 at 5 atm, and 8.5 at 10 atm.

We next explain the higher burning rates of *n*-hexane relative to mono-alkylated cyclohexanes. As seen in Fig. 10, there are more propene and less 1,3-butadiene in the flames of *n*-hexane compared to those in the flames of methylcyclohexane, the effect of which contradicts with their overall burning rates. However, we note that there is also considerably more C_2H_4 in the flames of *n*-hexane. C_2H_4 has notably high reactivity and high flame speeds seen in many previous measurements [3,31,32]. In addition, it is also found that in the flames of methylcyclohexane there are more intermediates with branched structure, which should be expected because methylcyclohexane itself includes a branched structure. Species with branched structure have been shown to have low reactivity, such as the laminar flame speeds of *iso*-butane versus *n*-butane [3,26], *iso*-butanol versus *n*-butanol [33], and *iso*-octane versus *n*-octane [17,34].

4.4. Ring structure on fuel cracking

By attributing the higher flame speed of cyclohexane to the fact that it cracks into less C_3 intermediates, we next discuss the reason as why it is so and why mono-alkylated cyclohexanes behave differently. The phenomenon can be explained by the β-scission rule, which is largely applicable in the high-temperature decomposition of radicals [35]. The β-scission rule states that the C—C bond that most like breaks is one position removed from the radical site. Figs. 11 and 12 show the reaction path for the ring opening and subsequent cracking of cyclohexane and methylcyclohexane under the dominant rule of β-scission. As shown in Fig. 11, due to the symmetric structure of the

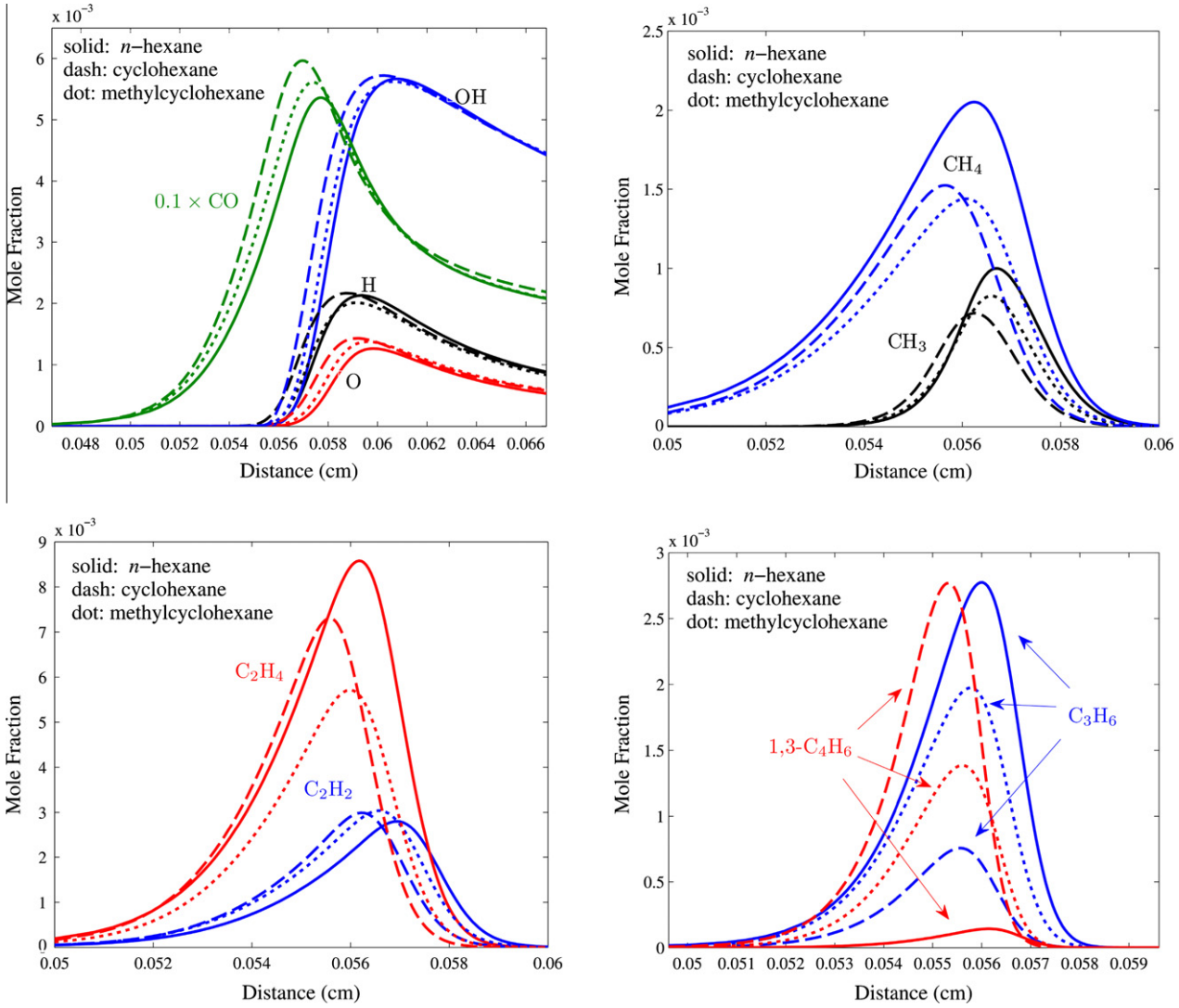

Fig. 10. Profiles of major C_0–C_4 intermediate fragments in the 1-D flames of *n*-hexane/air, cyclohexane/air and methylcyclohexane/air mixtures, at P = 10 atm, ϕ = 1.0, unburned gas temperature of 353 K, calculated with JetSurF 2.0 mechanism [15].

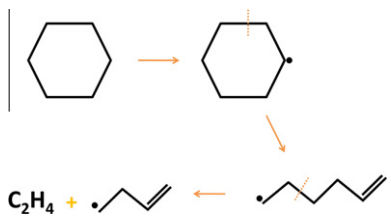

Fig. 11. Initial ring opening and subsequent cracking of cyclohexane at high temperature assuming the rule of β-scission dominates fuel cracking.

cyclohexane molecule, ring opening of cyclohexyl radical via β-scission occurs in two identical places, leading to the same intermediate: CH_2═CH—CH_2—CH_2—CH_2—CH_2^*. According to the β-scission rule, the radical CH_2═CH—CH_2—CH_2—CH_2-CH_2^* also undergo chain breaking at only one position because the radical site is at the end, which produces C_2H_4 and a CH_2═CH—CH_2—CH_2^* radical. It is therefore seen that the decomposition of cyclohexane clearly favors C_2 and C_4 over the C_3 fragments according to the β-scission rule.

On the other hand, the ring opening and subsequent cracking of methylcyclohexane and ethylcyclohexane is rather complicated

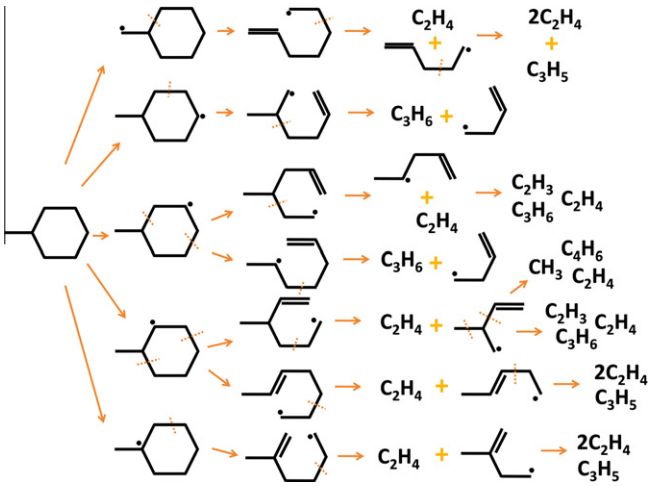

Fig. 12. Initial ring opening and subsequent cracking of methylcyclohexane at high temperature assuming the rule of β-scission dominates fuel cracking.

because the presence of the alkyl group breaks the symmetry and leads to a branched carbon structure. For methylcyclohexane, there are five isomers of methylcyclohexyl radicals, differentiated by their positions relative to the methyl group. Having the five isomers, even assuming the dominant β-scission rule, as shown in Fig. 12 there are still various possible ways of ring opening and subsequent cracking, leading to various C_3, straight C_4 and branched C_4 fuel intermediates. Indeed, as shown in Fig. 10, the distribution of C_3–C_4 intermediates in the flames of methylcyclohexane is more balanced compared to those in the flames of *n*-hexane and cyclohexane.

Admittedly, there are reactions other than β-scission, such as isomerization, dehydrogenation, addition, *etc.* However, since the purpose here is to identify the dominant factor explaining the higher reactivity of cyclohexane, other type of reactions are not plotted in Figs. 11 and 12. Detailed reaction path for cyclohexane and methylcyclohexane can be found in [6,9]. From the detailed reaction path for cyclohexane, it is seen that the radical $CH_2{=}CH{-}CH_2{-}CH_2{-}CH_2{-}CH_2^*$ can also undergo an important isomerization reaction, producing the $CH_2{=}CH{-}CH^*{-}CH_2{-}CH_2{-}CH_3$ radical. However, the new radical $CH_2{=}CH{-}CH^*{-}CH_2{-}CH_2{-}CH_3$ also has only one option for further β-scission due to the presence of the double bond, which produces 1,3-butadiene and $C_2H_5^*$. This further explains the higher reactivity of cyclohexane.

5. Conclusions

Using expanding spherical flames, laminar flame speeds for cyclohexane, methylcyclohexane and ethylcyclohexane were determined at atmospheric and elevated pressures up to 20 atm, and unburned gas temperature of 353 K. The resulting data at atmospheric pressure show reasonably good agreement with the measurements of Ji et al. [6]. Predictions of JetSurF 2.0 yield satisfactory agreement with the present data for all three fuels at all pressures, with slight over-prediction at atmospheric pressure.

The present measurements show the following trend for laminar flame speeds: cyclohexane > *n*-hexane > methylcyclohexane ≈ ethylcyclohexane at all pressures, thereby confirming and extending the trend found by Ji et al. [6] at atmospheric pressure to elevated pressures. The present results also show that the difference in flame speeds between the four fuels increases with pressure, with the maximum difference between the four fuels being approximately 5% at 1 atm and 13% at 10 atm.

Numerical tests show that while the difference in adiabatic flame temperatures between *n*-hexane and cyclohexane can explain their difference in flame speeds at atmospheric pressure, it cannot explain their difference in flame speeds at elevated pressures, which is shown to result from kinetic effects. Since cyclohexane and mono-alkylated cyclohexanes have identical adiabatic flame temperatures, the difference between their flame speeds is also due to kinetic effects.

Examination of the computed flame structures and rate constant sensitivity analysis show that the relative high reactivity of cyclohexane is mainly due to the fact that it decomposes into substantially more chain-branching 1,3-butadiene and less chain-terminating propene, owing to its symmetric ring structure and the general applicability of the β-scission rule. However, because of the presence of the alkyl group, methylcyclohexane and ethylcyclohexane crack into a more balanced distribution of intermediates, which bring their reactivity close to that of *n*-hexane.

Acknowledgments

This research was supported by the Air Force Office of Scientific Research under the technical monitoring of Dr. Julian M. Tishkoff. It is a pleasure to acknowledge helpful discussions with Yuxuan Xin and Dr. Peng Zhang.

References

[1] A. Violi, S. Yan, E.G. Eddings, A.F. Sarofim, S. Granata, T. Faravelli, E. Ranzi, Combust. Sci. Technol. 174 (2002) 339–417.
[2] M. Colket, T. Edwards, S. Williams, N.P. Cernansky, D.L. Miller, F.N. Egolfopoulos, et al., Development of an Experimental Database and Kinetic Models for Surrogate Jet Fuels, American Institute of Aeronautics and Astronautics Paper, No. 2007-770.
[3] S.G. Davis, C.K. Law, Combust. Sci. Technol. 140 (1998) 427–449.
[4] J.T. Farrell, R.J. Johnston, I.P. Androulakis, Molecular Structure Effects on Laminar Burning Velocities at Elevated Temperature and Pressure, Society of Automotive Engineers Paper, No. 2004-01-2936.
[5] T. Dubois, N. Chaumeix, C.-E. Paillard, Energy Fuels 23 (2009) 2453–2466.
[6] C. Ji, E. Dames, B. Sirjean, H. Wang, F.N. Egolfopoulos, Proc. Combust. Inst. 33 (2011) 971–978.
[7] W.J. Pitz, N.P. Cernansky, F.L. Dryer, F.N. Egolfopoulos, J.T. Farrell, D.G. Friend, Development of an Experimental Database and Chemical Kinetic Models for Surrogate Gasoline Fuels, Society of Automotive Engineers Paper, No. 2007-01-0175.
[8] J.T. Farrell, N.P. Cernansky, F.L. Dryer, D.G. Friend, C.A. Hergart, C.K. Law, et al., Development of an Experimental Database and Kinetic Models for Surrogate Diesel Fuels, Society of Automotive Engineers Paper, No. 2007-01-0201.
[9] S. Granata, T. Faravelli, E. Ranzi, Combust. Flame 132 (2003) 533–544.
[10] C. Cavallotti, R. Rota, T. Faravelli, E. Ranzi, Proc. Combust. Inst. 31 (2007) 201–209.
[11] E. Ranzi, Energy Fuels 20 (2006) 1024–1032.
[12] P. Dagaut, M. Cathonnet, Prog. Energy Combust. Sci. 32 (2006) 48–92.
[13] E.J. Silke, W.J. Pitz, C.K. Westbrook, M. Ribaucour, J. Phys. Chem. A 111 (2007) 3761–3775.
[14] W.J. Pitz, C.V. Naik, T.N. Mhaoldúin, C.K. Westbrook, H.J. Curran, J.P. Orme, et al., Proc. Combust. Inst. 31 (2007) 267–275.
[15] H. Wang, E. Dames, B. Sirjean, D.A. Sheen, R. Tangko, A. Violi, et al., A High-temperature Chemical Kinetic Model of *n*-Alkane (up to *n*-Dodecane), Cyclohexane, and Methyl-, Ethyl-, *n*-Propyl and *n*-Butyl-Cyclohexane Oxidation at High Temperatures, University of Southern California, 2010.
[16] C. Ji, E. Dames, Y.L. Wang, H. Wang, F.N. Egolfopoulos, Combust. Flame 157 (2010) 277–287.
[17] A.P. Kelley, A.J. Smallbone, D.L. Zhu, C.K. Law, Proc. Combust. Inst. 33 (2011) 963–970.
[18] A.P. Kelley, A.J. Smallbone, D.L. Zhu, C.K. Law, Experimental Measurement of *n*-Pentane Flame Speeds at Elevated Pressures and Temperatures, 6th US National Combustion Meeting, 2009.
[19] A.P. Kelley, J.K. Bechtold, C.K. Law, Confined Propagation of Premixed Flames, 7th U.S. National Combustion Meeting, 2011.
[20] C.K. Wu, C.K. Law, Proc. Combust. Inst. (1984) 1941–1949.
[21] A.P. Kelley, C.K. Law, Combust. Flame 156 (2009) 1844–1851.
[22] G.H. Markstein, J. Aeronaut. Sci. 18 (1951) 199–209.
[23] A.P. Kelley, G. Jomaas, C.K. Law, Combust. Flame 156 (2009) 1006–1013.
[24] M.P. Burke, Z. Chen, Y. Ju, F.L. Dryer, Combust. Flame 156 (2009) 771–779.
[25] Z. Chen, M.P. Burke, Y. Ju, Proc. Combust. Inst. 32 (2009) 1253–1260.
[26] A.P. Kelley, Dynamics of Expanding Flames, Ph.D. Thesis, Princeton University, 2011.
[27] R.J. Kee, J.F. Grcar, M.D. Smooke, J.A. Miller, E. Meeks, Premix: a Fortran Program for Modeling Steady Laminar One-dimensional Premixed Flames. Sandia Report 85-8240, 1985.
[28] A.J. Smallbone, W. Liu, C. Law, X. You, H. Wang, Proc. Combust. Inst. 32 (2009) 1245–1252.
[29] K. Kumar, J.E. Freeh, C.J. Sung, Y. Huang, J. Propul, Power 23 (2007) 428–436.
[30] X. You, F.N. Egolfopoulos, H. Wang, Proc. Combust. Inst. 32 (2009) 403–410.
[31] G. Jomaas, X.L. Zheng, D.L. Zhu, C.K. Law, Proc. Combust. Inst. 30 (2005) 193–200.
[32] F. Wu, A.P. Kelley, C. Tang, D.L. Zhu, C.K. Law, Int. J, Hydrogen Energy (2011) 1–10.
[33] W. Liu, A.P. Kelley, C.K. Law, Proc. Combust. Inst. 33 (2011) 995–1002.
[34] A.P. Kelley, W. Liu, Y.X. Xin, A.J. Smallbone, C.K. Law, Proc. Combust. Inst. 33 (2011) 501–508.
[35] C.K. Law, Combustion Physics, Cambridge University Press, 2006.